Electronic Supplementary Information

Three-dimensional amorphous tungsten-doped nickel phosphide microsphere as an efficient electrocatalyst for hydrogen evolution

Zhaoyu Jin, Panpan Li, Xing Huang, Guangfeng Zeng, Yong Jin,* Baozhan Zheng, and Dan Xiao*

Contents:

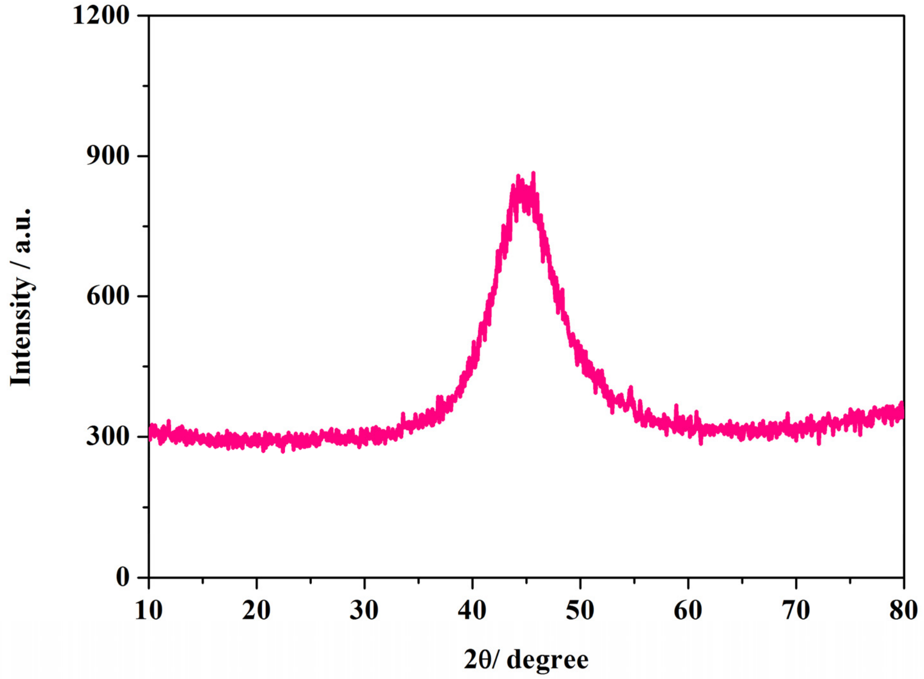

Fig. S1. XRD pattern of a-WNP. a typical wide peak is exhibited assigned to the amorphous structure of a-WNP.

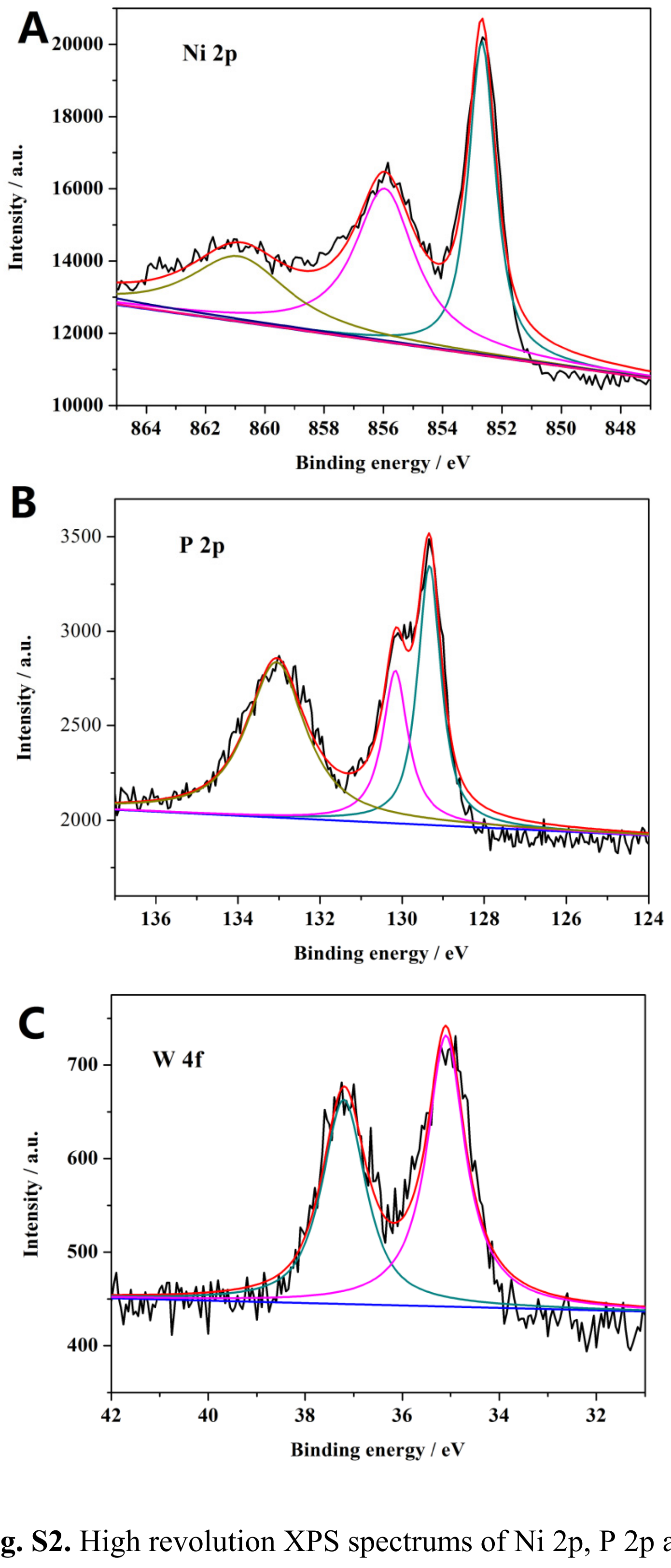

Fig. S2. High revolution XPS spectrums of Ni 2p, P 2p and W 4f.

The onset-potential for HER was obtained from Tafel plot.[1] For exmple, the semi-log plot of a-WNP in the region of low current densities as shown in Fig. S3 shows a linear relationship below - 51 mV but starts to deviate above - 49 mV. Therefore, -50 mV was chosen as the onset potential for a-WNP. The same method was applied on determining the overpotential for other samples in the paper.

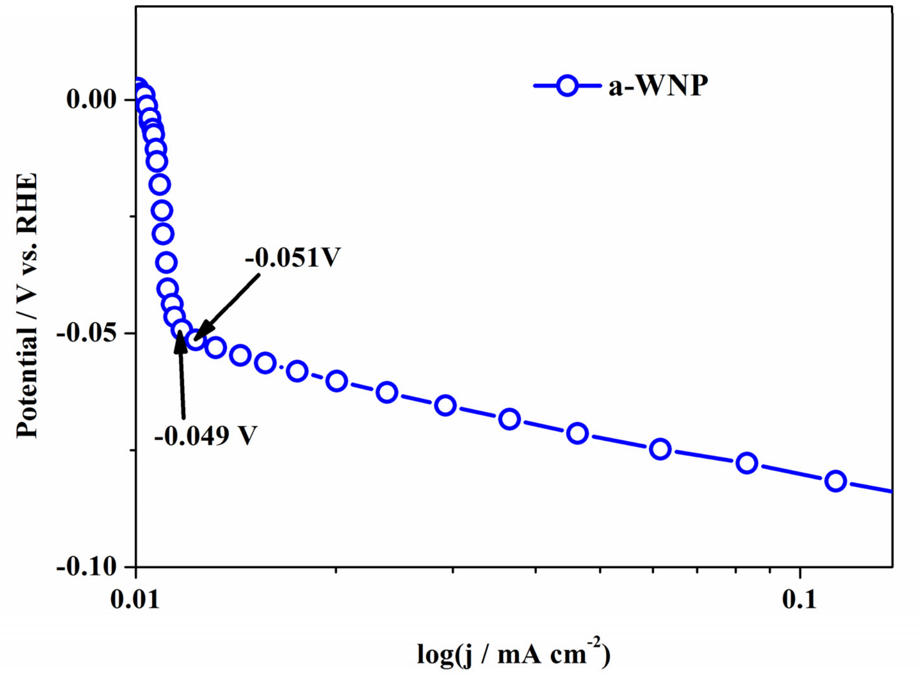

Fig. S3. The Tafel plot of a-WNP in the region of low current densitiy.

Table S1. A summarized comparison of some reported HER catalysts and a-WNP in acidic electrolyte.

Catalyst	**η(mV)@5 mA cm^{-2}**	**η(mV)@20 mA cm^{-2}**	**Tafel slope(mVdec^{-1})**	**Reference**
Ni_2P	110	130	46	2
MoS_2/rGO	130	170	41	3
Ni/NiO/$CoSe_2$ nanocomposite	90	140	39	4
defect-rich MoS_2 nanosheets	170	210	50	5
WS_2/rGO	240	280	58	6
MoP network	110	150	54	7
MoS_x/graphene/Ni foam	120	160	43	8
MoP	125	160	53	9
a-WNP	75	110	39	**This work**

Determine of the turnover frequency (TOF):

The number of active sites was firstly taken into account and obtained as follow: CV measurements were carried out in neutral PBS solution (pH = 7). Then, the absolute components of the voltammetric charges (cathodic and anodic) reported during one single blank measurement was added. Assuming a one electron redox process, this absolute charge was divided by two. The value was then divided by the Faraday constant to get the number of active sites (*n*) of the a-WNP electrode.

The TOF(s^{-1}) was calculated following equation:

TOF = I/2nF

where I is the current (A) during the LSV measurement in 0.5 M H_2SO_4, F is Faraday constant (96485 C mol^{-1}) and *n* is the number of active sites (mol). The factor 1/2 arrives by taking into account that two electrons are required to form one hydrogen molecule from two protons.[10, 11]

The electrochemical active surface area (EASA) was calculated according to the he electrochemical double-layer capacitance with a blank glassy carbon electrode (GCE) as reference. EASA of GCE was obtained using the following equation: [12]

$i_p = 0.4463 \times 10^{-3} \times n^{3/2} \times F^{3/2} \times A \times C_R^{*} \times D^{1/2} \times v^{1/2} \times (RT)^{-1/2}$

where n is the number of electrons transferred (ferrocyanide, n=1), F is Faraday's constant (96485 C mol^{-1}), R is the gas constant (8.314 J mol^{-1} K^{-1}), T is the temperature (298 K), $CR*$ (mol L^{-1}) is the initial ferrocyanide concentration, and v is the CV scan rate (0.05 V s-1). The diffusion coefficient (DR) of ferrocyanide was based on reference data[12] (3.7 × 10^{-6} cm^2 s^{-1}), and the calculated EASA of the GCE was 0.2 cm^2.

The EASA of the porous N/C electrodes was calculated using a double-layer capacitor in Fig. S4 and the following equation: [13]

$C = A \times (\varepsilon_r \times \varepsilon_0) / d = (\int I \times dV) / v \times m \times V$

where ε_r is the electrolyte dielectric constant, ε_0 is the dielectric constant of the vacuum, d is the effective thickness of the double layer (charge separation distance), A is the EASA, I is the response current density, V is the potential (V), v is the potential scan rate, and m is the mass of the catayst in the electrodes. the EASA of Ni_xP based electrode can be calculated using the equation: $A_1/A_2=C_1/C_2$ (A_1 is EASA of glassy carbon electrode, and A_2 is EASA of the catalyst modified electrode). The results are summarized in Table S2.

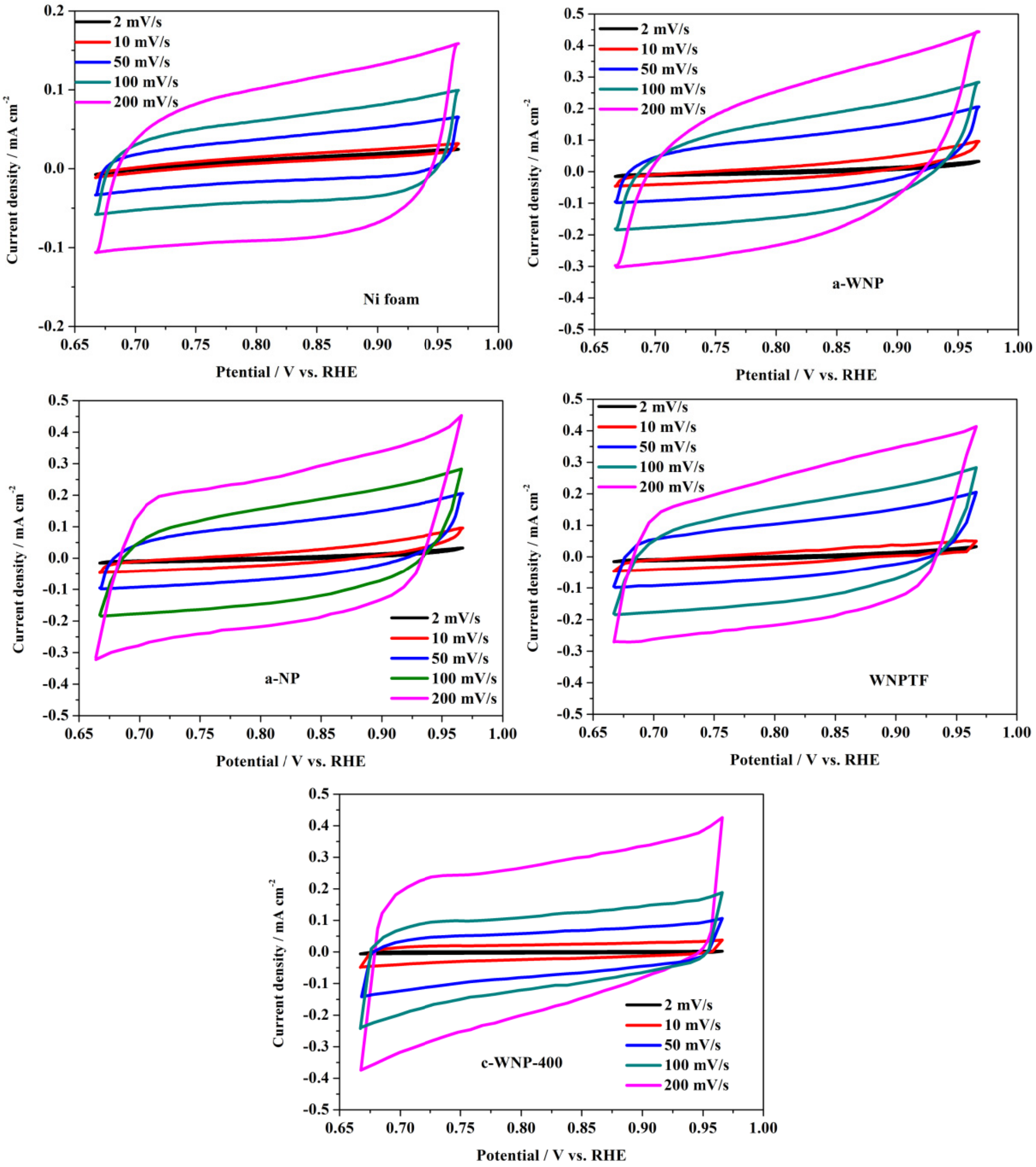

Fig. S4. cyclic voltammograms of above catalysts at different scan rates of 2, 10, 50, 100 and 200 mV s^{-1} in 0.1 M KOH.

Table S2. Calculated EASA of the four catalysts.

catalyst	EASA (m^2 g^{-1})
WNPTF	9
a-NP	17
c-WNP-400	13.5
a-WNP	15

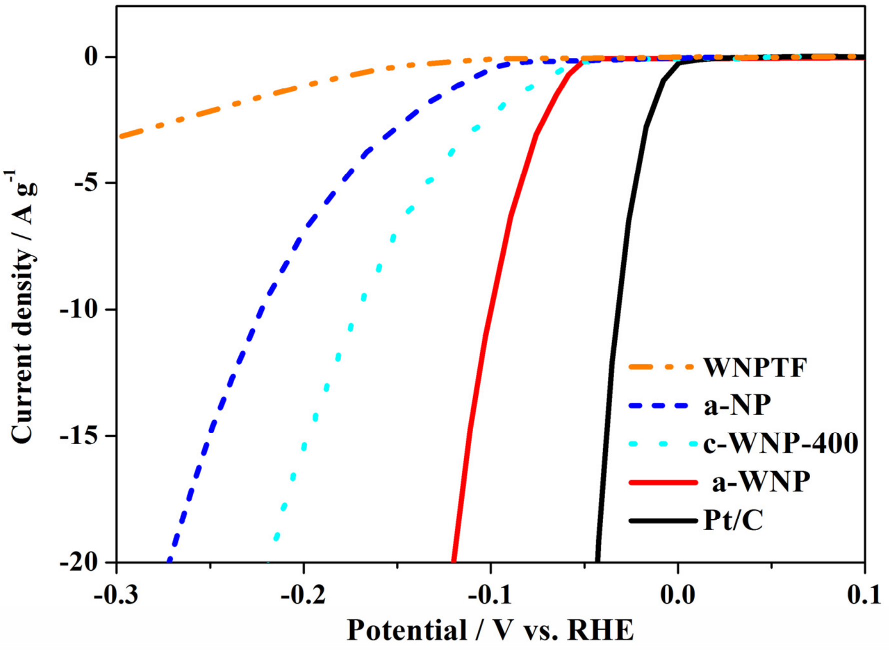

Fig. S5. Polarization curves of the catalysts in 0.5 M H_2SO_4; the current densities are normalized by the mass loading.

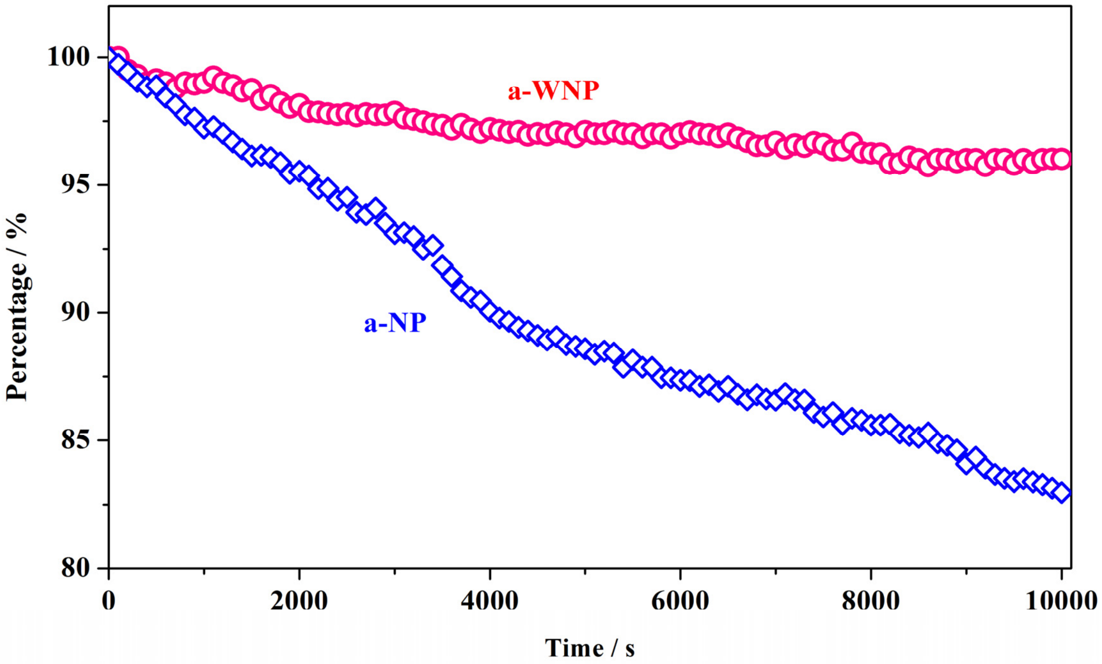

Fig. S6. Steady-state chronoamperometric curve of a-WNP and a-NP for 10000 s at an applied potential of - 0.1 V vs. RHE in 0.5 M H_2SO_4.

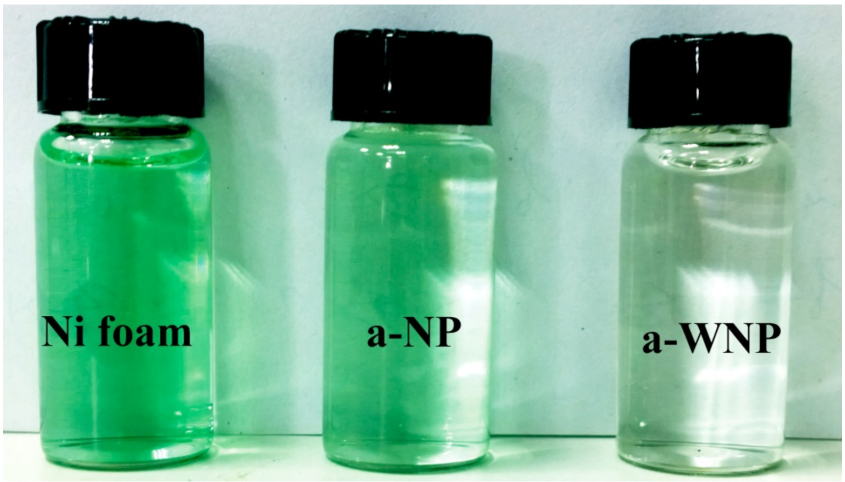

Fig. S7. An optical photograph of the collected H_2SO_4 electrolyte after sweeping between - 0.2 V to + 0.2 V for 1000 cycles by using the above three electrode as anode.

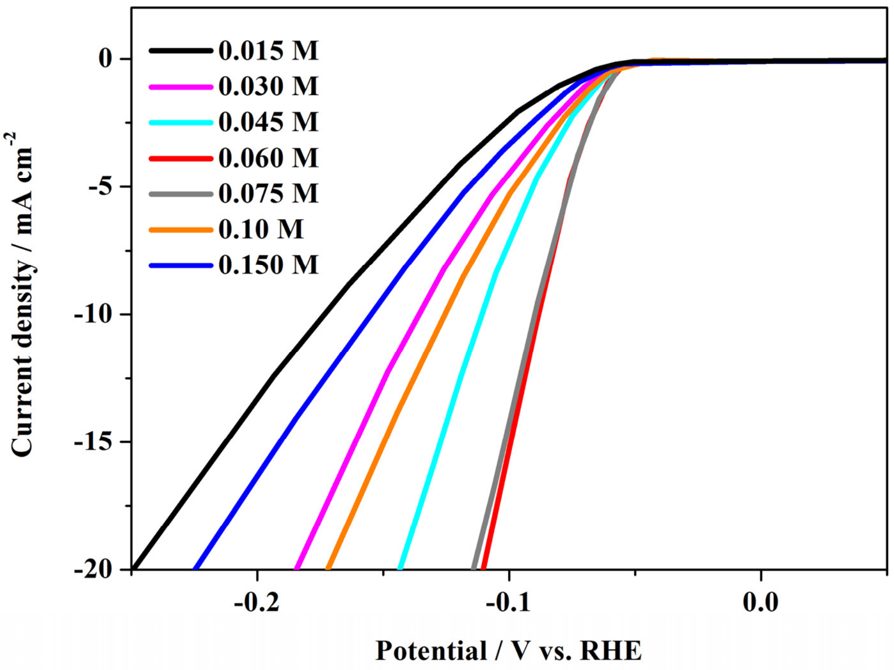

Fig. S7. Polarization curves of the a-WNP in different content of W.

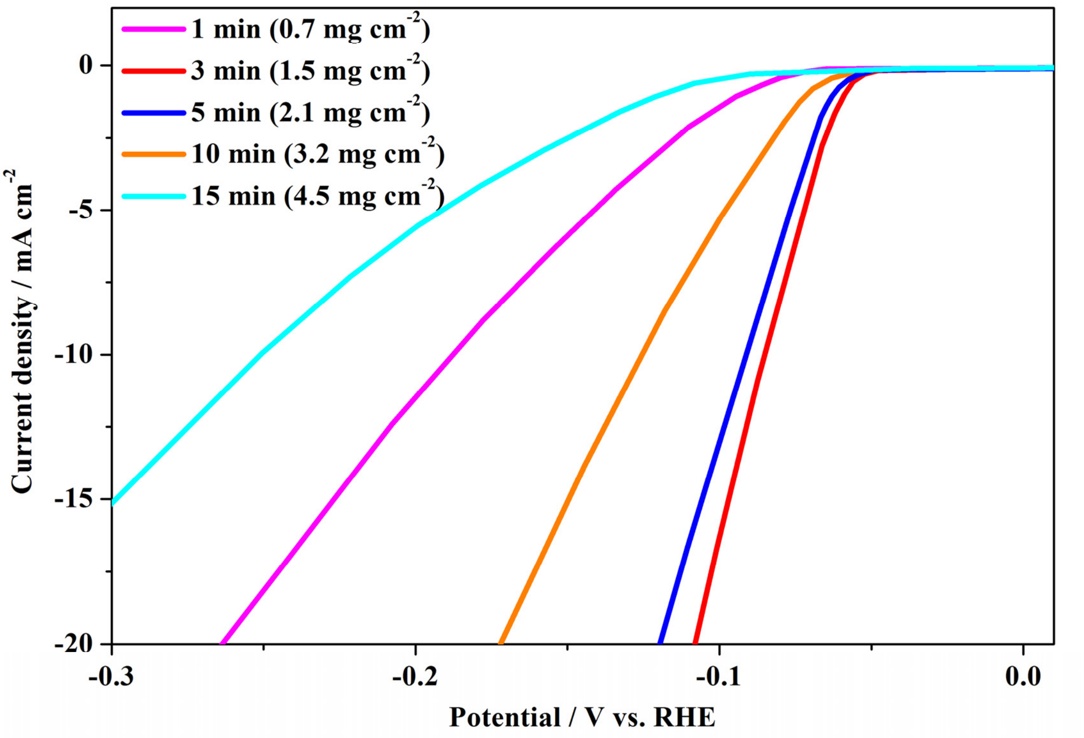

Fig. S8. Polarization curves of the a-WNP deposited for different length of time, the current densities are normalized by the geometrical area.

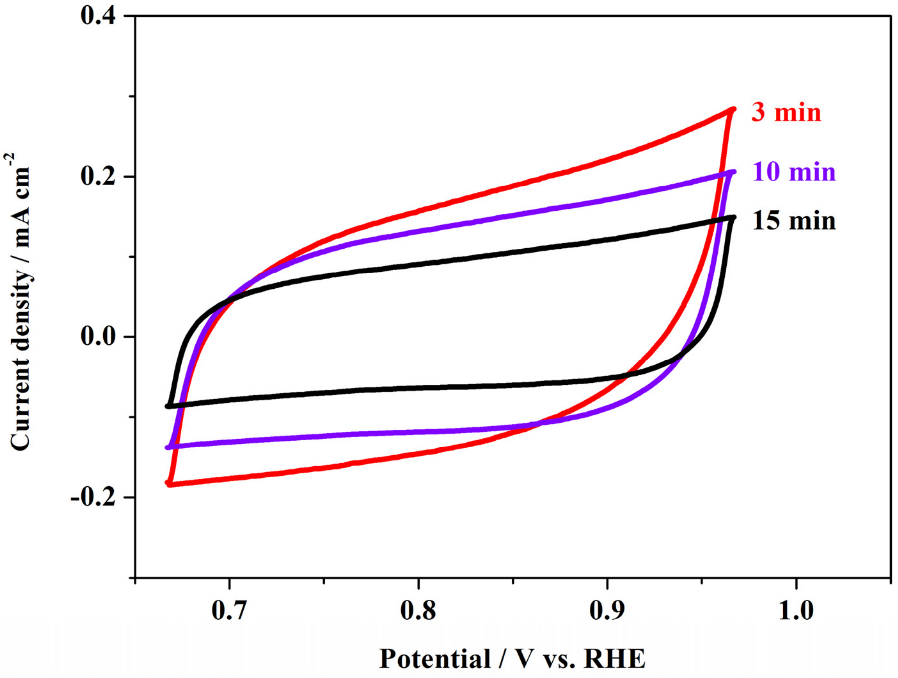

Fig. S9. CVs of the a-WNP deposited on Ni foam for 3, 10 and 15 min in 0.1 M KOH with a scan rate of 100 mV s^{-1}. The decrease of electrochemical double-layer charged current density with the extend of the reaction time indicates a decline of EASA.

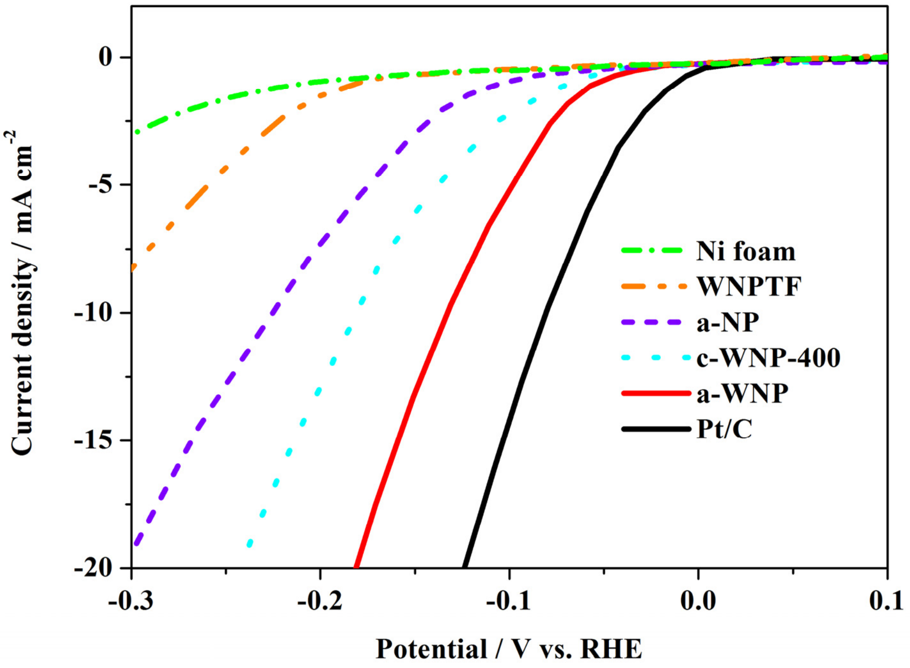

Fig. S10. Polarization curves of the Ni foam, WNPTF, a-NP, c-WNP-400, a-WNP and Pt/C catalysts in 1.0 M KOH.

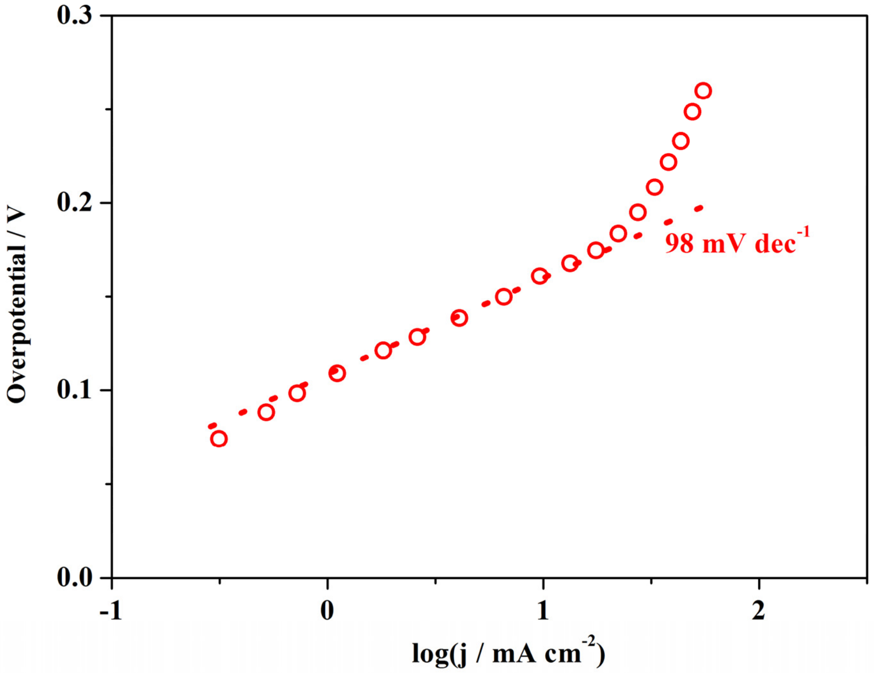

Fig. S11. Tafel plot of a-WNP in1.0 M KOH.

Table S3. Comparison of HER performance in alkaline media for a-WNP with other HER electrocatalysts.

catalyst	η(mV)@5 mA cm^{-2}	η(mV)@20 mA cm^{-2}	Tafel slope($mVdec^{-1}$)	Reference
Mo_2C	170	210	54	14
MoB	210	240	59	14
Ni_2P	150	200	-	2
Co_2P	200	250	129	10
a-WNP	110	180	98	this work

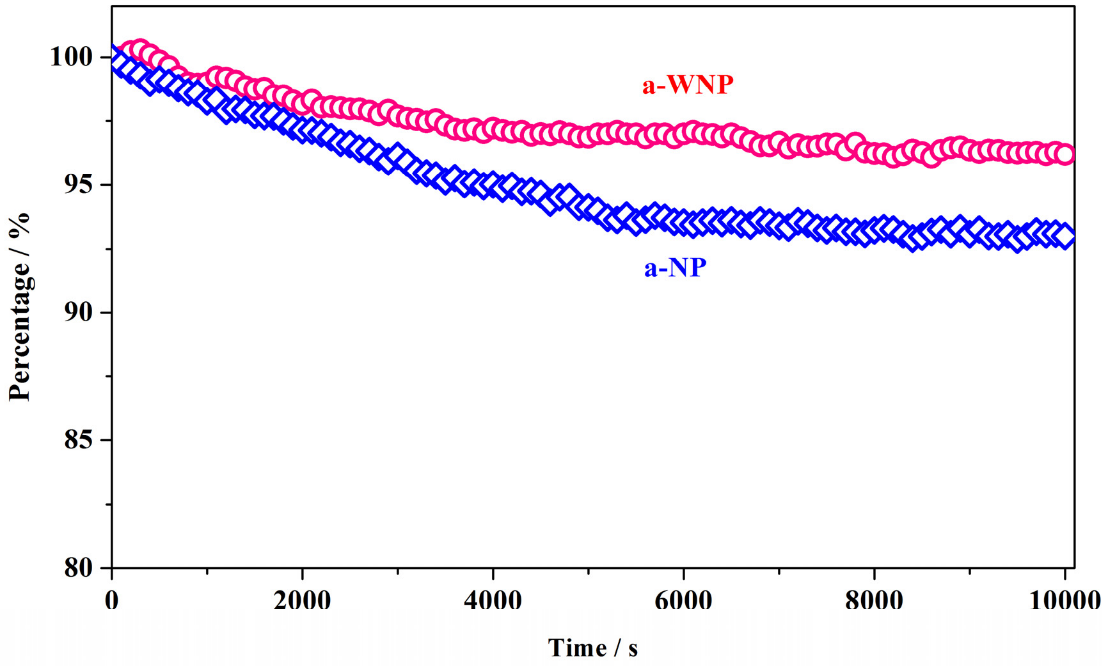

Fig. S11. Steady-state chronoamperometric curve of a-WNP and a-NP for 10000 s at an applied potential of - 0.1 V vs. RHE in 1.0 M KOH.

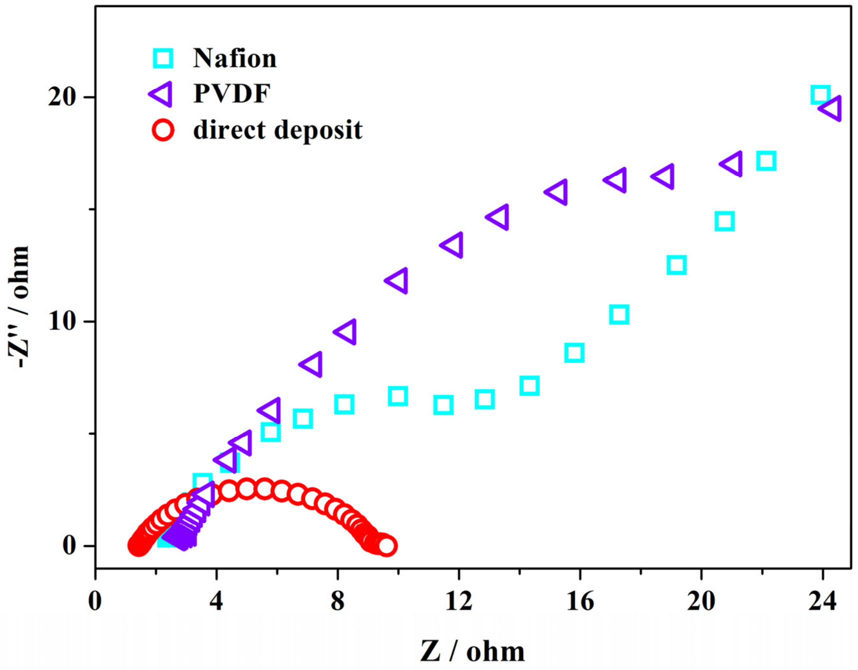

Fig. S12. EIS spectra of the a-WNP modified electrode with the binder of Nafion, PVDF and binder-free direct deposit at the overpotential of 0.2 V.

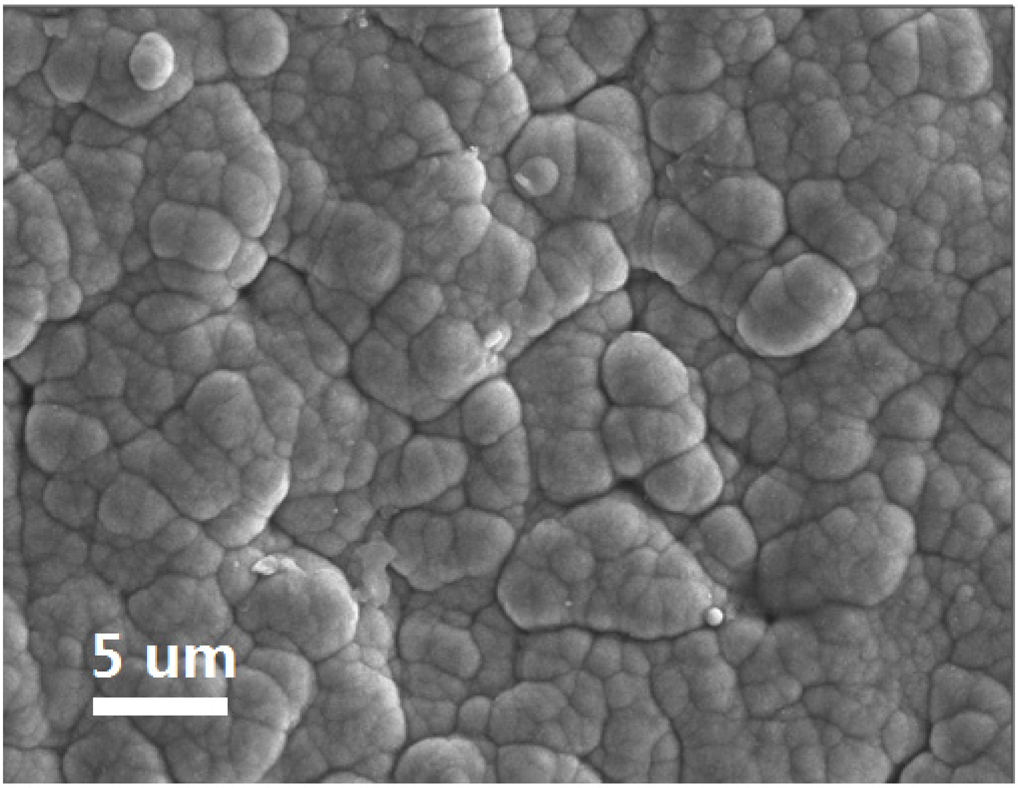

Fig. S13. SEM image of WNPTF on Ni foam. The dense films could be observed which lead to the decrease of specific area and less active sites exposed to catalyze hydrogen generation.

References:

S

1. Y. Zhao, K. Kamiya, K. Hashimoto and S. Nakanishi, *Angew. Chem. Int. Ed.*, 2013, **52**, 13638-13641.
2. E. J. Popczun, J. R. McKone, C. G. Read, A. J. Biacchi, A. M. Wiltrout, N. S. Lewis and R. E. Schaak, *J. Am. Chem. Soc.*, 2013, **135**, 9267-9270.
3. Y. Li, H. Wang, L. Xie, Y. Liang, G. Hong and H. Dai, *J. Am. Chem. Soc.*, 2011, **133**, 7296-7299.
4. Y. F. Xu, M. R. Gao, Y. R. Zheng, J. Jiang and S. H. Yu, *Angew. Chem. Int. Ed. Engl.*, 2013, **52**, 8546-8550.
5. J. Xie, H. Zhang, S. Li, R. Wang, X. Sun, M. Zhou, J. Zhou, X. W. Lou and Y. Xie, *Adv. Mater.*, 2013, **25**, 5807-5813.
6. J. Yang, D. Voiry, S. J. Ahn, D. Kang, A. Y. Kim, M. Chhowalla and H. S. Shin, *Angew. Chem. Int. Ed.*, 2013, **52**, 13751-13754.
7. Z. Xing, Q. Liu, A. M. Asiri and X. Sun, *Adv. Mater.*, 2014.
8. Y. H. Chang, C. T. Lin, T. Y. Chen, C. L. Hsu, Y. H. Lee, W. J. Zhang, K. H. Wei and L. J. Li, *Adv. Mater.*, 2013, **25**, 756-760.
9. P. Xiao, M. A. Sk, L. Thia, X. Ge, R. J. Lim, J.-Y. Wang, K. H. Lima and X. Wang, *Energy Environ. Sci.*, 2014.
10. J. Q. Tian, Q. Liu, A. M. Asiri and X. P. Sun, *J. Am. Chem. Soc.*, 2014, **136**, 7587-7590.
11. D. Merki, S. Fierro, H. Vrubel and X. L. Hu, *Chem. Sci.*, 2011, **2**, 1262-1267.
12. Y. X. Huang, X. W. Liu, J. F. Xie, G. P. Sheng, G. Y. Wang, Y. Y. Zhang, A. W. Xu and H. Q. Yu, *Chem. Commun.*, 2011, **47**, 5795-5797.
13. J. Yan, T. Wei, B. Shao, F. Q. Ma, Z. J. Fan, M. L. Zhang, C. Zheng, Y. C. Shang, W. Z. Qian and F. Wei, *Carbon*, 2010, **48**, 1731-1737.
14. H. Vrubel and X. L. Hu, *Angew. Chem. Int. Ed.*, 2012, **51**, 12703-12706.